Catal Lett (2008) 121:39–51
DOI 10.1007/s10562-007-9289-0

Selective Oxidation of Ethane Over Mo–V–Al–O Oxide Catalysts: Insight to the Factors Affecting the Selectivity of Ethylene and Acetic Acid and Structure-activity Correlation Studies

T. M. Sankaranarayanan · R. H. Ingle · T. B. Gaikwad · S. K. Lokhande · T. Raja · R. N. Devi · V. Ramaswamy · P. Manikandan

Received: 12 July 2007 / Accepted: 15 September 2007 / Published online: 12 October 2007

Abstract Catalysts of general formula, $MoVAlO_x$ were prepared with the initial elemental composition of 1:0.34:0.167 (Mo:V:Al) at a pH value in the range of 1–4. The elemental analysis showed that the final composition of the catalysts is pH dependant. The performance of the catalysts was tested for selective oxidation of ethane to give ethylene and acetic acid. While all of them were active for ethane oxidation with a moderate conversion, the catalyst prepared at pH 2 showed a highest activity with 23% ethane conversion and a combined selectivity of 80.6% to ethylene and acetic acid. The catalyst prepared at pH 4 was least selective to ethylene and acetic acid. Various techniques like powder XRD, SEM, Raman, UV–Vis and EPR were used to characterize the catalysts and to identify the active phases responsible for the selective oxidation of ethane. The powder XRD data showed that the catalysts prepared at pH 1 and 2 contain mainly of MoO_3 and MoV_2O_8 along with traces of Mo_4O_{11}. The amount of MoO_3 was slightly higher in the catalyst prepared at pH 1. However, the catalyst prepared at pH 3 contains mainly of MoV_2O_8 with no trace of MoO_3. The catalyst prepared at pH 4 showed V_2O_5 as the major phase along with $MoVAlO_4$ phase. The Raman data corroborated the XRD results. EPR and UV–Vis studies indicated the presence of traces of V^{4+} in pH 1 and 2 catalysts and significant amount of Mo^{5+} in all the catalysts. Thus, the high activity and selectivity to ethylene and acetic acid are attributed to the presence of MoV_2O_8 phase and other reduced species like Mo_4O_{11} phase supported on MoO_3. The presence of V and Mo ions in a partially reduced form seems to play a crucial role in the selective oxidation of ethane.

Keywords Ethane · Selective oxidation · Acetic acid · Ethylene · Mixed metal oxide

1 Introduction

Research activities on the selective oxidation of lower alkanes, especially C_2–C_4 alkanes, to the corresponding alkenes or oxygenates (acetic acid, acrylic acid, etc.) have gained a high momentum in recent years [1, 2]. Selective oxidation of lower alkanes is an attractive path towards the chemical utilization of cheap natural gas resources. One-step direct oxidation of ethane and propane to acetic acid and acrylic acid, respectively, is an alternative method to the currently employed alkene based routes [2–5]. Generally, lower alkanes are less reactive due to the non-availability of a lone pair electrons and little polarity of the C–H bonds, and hence, their oxidation is usually encountered with many difficulties. Furthermore, a high selectivity to the required products is generally obtained at low conversions. Higher conversions invariably lead to less selective products, due to the formation of thermodynamically stable, undesirable combustion products. In spite of the above limitation, a great deal of efforts have been attempted to achieve selective functionalization of lower alkanes. However, in the case of selective oxidation of ethane only a few catalysts are known that are efficient in terms of acetic acid and ethylene yield at a relatively mild experimental condition [1, 2, 6].

The oxidation of ethane involves several micro intermediate steps that require a multifunctional catalyst. Thus,

T. M. Sankaranarayanan · R. H. Ingle · T. B. Gaikwad · S. K. Lokhande · T. Raja · R. N. Devi · V. Ramaswamy · P. Manikandan (✉)
Catalysis and Inorganic Chemistry Division, National Chemical Laboratory, Dr. Homi Bhabha Road, Pune 411 008, India
e-mail: palanimani@yahoo.com

the selection of a suitable catalyst containing many active phases (multifunctionality) for the ethane oxidation and under appropriate operating condition to maximize the selectivity to ethylene and/or acetic acid is a complex and challenging task. Several research groups have studied a broad spectrum of catalysts using various techniques to understand the active sites responsible for the selective oxidation of ethane. However, the knowledge available on the reaction mechanism is still rather limited and hence there is a need for systematic studies on the wide range of catalyst systems in order to understand the structure-activity correlations [2, 7, 8].

There have been many reports emphasizing the importance of elements like Te and Nb ions along with the basic composition containing Mo–V for the formation/stabilization of the active phases responsible for the selective oxidation of ethane [1, 5, 9, 10]. Reports are also available indicating the importance of the initial elemental composition, the pH, the preparation methodologies and the treatment temperatures for a better yield of the required alkenes and oxygenates, however, these dependencies vary catalyst to catalyst [4, 6].

The initial report on $MoVAlO_x$ by Ueda et al at atmospheric pressure and at 340 °C showed <4 mol% ethane conversion with a low selectivity to acetic acid [11]. In the present paper, we report on the catalytic activity of $MoVAlO_x$ type catalysts for the selective oxidation of ethane to produce ethylene and acetic acid at moderate ethane conversion, as a function of the pH of the preparative gel of the catalysts synthesized. $MoVAlO_x$ type catalysts prepared at different pH conditions were also tested at different experimental conditions viz. pressure, temperature and ethane/O_2/H_2O feed ratios in order to obtain acetic acid and ethylene in high yield. Interestingly, the catalyst prepared from a gel at pH 2 was found to have superior activity than other catalysts. We have also identified different phases present in the catalysts prepared at different pH conditions. A structure-activity correlations were made based on the detailed characterization of the catalysts by XRD, Raman, UV–Vis and EPR spectral techniques.

2 Experimental

2.1 Catalyst Preparation and Characterization

Catalyst composition of general formula $MoVAlO_x$ with a preparative composition of the elements Mo, V, and Al in the atomic ratio 1:0.33:0.167 respectively was synthesized using a hydrothermal method [11]. Anderson-type heteropolymolybdate, $(NH_4)_3AlMo_6H_6O_{24} \cdot 7H_2O$, prepared from the mixed aqueous solution of ammonium heptamolybdate and aluminum sulfate [11, 12], was used as a source for Mo and Al. Typically, the catalyst compositions of $MoVAlO_x$ were prepared as follows: aqueous solutions of $(NH_4)_3AlMo_6H_6O_{24} \cdot 7H_2O$ and $VOSO_4$ were mixed at room temperature, the slurry was adjusted to the required pH value (1, 2, 3, and 4) using NH_4OH or HNO_3 and the final mixture was transferred to a PTFE lined autoclave (400 mL capacity). The autoclave was heated to 175 °C for 48 h under constant rotation (40 rpm). After 48 h, the autoclave was cooled and the dark solid mass obtained at the bottom of the autoclave was separated from the solution, washed with water several times and dried at 100 °C overnight in an oven. The final catalyst compositions were named as $MoVAlO_x$-1, $MoVAlO_x$-2, $MoVAlO_x$-3 and $MoVAlO_x$-4 where the numerical values indicate the pH at which the catalysts were prepared.

The bulk compositions of Mo, V and Al were analyzed by ICP using a Plasma 400 Perkin–Elmer spectrometer and their surface composition was done using EDX method. The surface area of the catalysts was determined by N_2 adsorption at 77 K, using the multipoint BET analysis method with an Autosorb-1 Quantachrome flow apparatus. The catalysts were dehydrated in vacuum at 250 °C for 10 h prior to the measurements. The room temperature powder X-ray diffraction (PXRD) patterns of calcined catalysts were collected on a Philips X′ Pert Pro 3040/60 diffractometer using Cu Kα radiation (l = 1.5418 Å), nickel filter and X'celerator as detector which employs the real time multiple strip (RTMS) detection technique. PXRD patterns were collected in the 2θ range 5–75° with steps of 0.017°. Scan type was the continuous scanning mode and scan time per step was 50 s. Scanning electron microscopy (SEM) and EDX microanalyses were performed on a JEOL JSM 6300 LINK ISIS instrument.

The IR and Raman spectra of the catalysts were recorded on a Shimadzu FT-IR 8201 PC instrument and Ranishaw 2000 Raman Microscope excited with 633 nm Laser respectively. Diffuse reflectance (DR) UV–Vis spectra were collected on a Perkin Elmer Lambda 900 series equipped with a 'Praying Mantis' attachment from Harrick. The spectra were recorded for $VOSO_4$, MoO_3, V_2O_5 and as-synthesized and calcined catalysts of $(NH_4)_3AlMo_6H_6O_{24} \cdot 7H_2O$ as references for the analysis. The electron paramagnetic resonance (EPR) spectra were recorded at room temperature on a Bruker EMX X-band spectrometer operating at 100 kHz field modulation. The microwave frequency was calibrated using a frequency counter of the microwave bridge ER 041 XG-D. Bruker Simfonia and WINEPR software packages were used in the spectral simulations and to calculate hyperfine coupling constant.

2.2 Catalytic Activity

The ethane oxidation experiments were performed in a typical laboratory fixed-bed reactor using a corrosion resistant stainless steel tubular reactor of internal diameter of 9 and 450 mm height which was kept in a tubular furnace. The catalyst (0.3–0.5 mm particle size) was introduced in the reactor and diluted with 2–4 g of silicon carbide with similar in size in order to keep a constant volume in the catalyst bed. A thermocouple was installed in the center of the catalyst bed in contact with the catalyst particles to measure the reaction temperature. The heating zones at the inlet and the outlet of the reactor were filled with inert porcelain particles. The catalyst was activated by heating the reactor to 350 °C at a heating rate of 2 °C/min under air flow for 4 h and then to 400 °C under He flow for 4 h. The reactor was then brought to the required temperature, and pressurized to the required level with a feed using a back-pressure controller placed on the reactor outlet stream. A typical composition of the feed was ethane/air/steam: 27.6/47.6/24.8 mol%. The water (steam) feed was pre-heated at 250 °C and then thoroughly mixed with the other gas feed prior to their contact with the catalyst. The flow rate was varied (from 40 to 100 mL/min) in order to achieve different ethane conversion levels. Experiments were carried out at temperatures in the range 250–350 °C to achieve the highest combined selectivity for ethylene and acetic acid at a moderate ethane conversion.

The liquid products (mainly acetic acid and water) were separated from the gas products by an ice cold condenser, collected in high pressure liquid–gas separator and analyzed using an off-line GC (HP 5890 series 11 using a 1.5 m by 3 mm column packed with material sold under the trademark PORAPAQ^{TM}. QS). Acetic acid was also estimated by standard volumetric titration method. The gas products were analyzed on-line by gas chromatography (Chemito GC1000) operating with three columns: oxygen, nitrogen and carbon monoxide were analyzed using a 2.5 m by 3 mm column of 13× molecular sieve. Carbon dioxide, ethane and ethylene were analyzed using a 0.5 m by 3 mm column packed with material sold under the trade name PORAPAQ^{TM}. N. The carbon balance was in the range 93–97%. In all cases, the conversion and selectivity calculations were based on the stoichiometry:

$$CH_3CH_3 + \tfrac{1}{2}O_2 \rightarrow CH_2 = CH_2 + H_2O;$$
$$CH_3CH_3 + 1\tfrac{1}{2}O_2 \rightarrow CH_3COOH + H_2O;$$
$$CH_3CH_3 + 2\tfrac{1}{2}O_2 \rightarrow 2CO + 3H_2O;$$
$$CH_3CH_3 + 3\tfrac{1}{2}O_2 \rightarrow 2CO_2 + 3H_2O.$$

The selectivity data were calculated on the basis of product sum. Details of the reaction conditions are described in the footnotes of the tables and figures. The conversion of ethane in an experiment using an empty-volume reactor (blank run) was lower than 1%, confirming that the homogeneous reaction is negligible at the experimental conditions employed for the present catalytic activities.

3 Results

3.1 Synthesis and Characterization

3.1.1 Synthesis, Elemental Composition and Surface Properties

The elemental composition of catalysts of general formula $MoVAlO_x$ prepared hydrothermally at four different pH values and the yield of the final catalysts (calcined catalysts) are given in Table 1. The catalyst yield was found to decrease at higher pH condition as seen in the Table 1. The bulk elemental composition of the catalysts was obtained from ICP analysis. The data clearly indicate that the final composition of the catalyst is different from the initial preparative composition depending on the pH values. Also, Mo/V and Mo/Al molar ratios decrease with increase in pH indicating that the Mo content is lower at the higher pH value.

The surface elemental composition for all the catalysts was determined by EDX method (Table 1) and it was found that these elemental compositions are different from the bulk composition. The amount of vanadium at the surface of the catalysts was higher as compared to that of

Table 1 Elemental compositions and surface properties of hydrothermally synthesized $MoVAlO_x$ catalysts prepared at different pH values

Catalyst	Catalyst yield,[a] %	Composition		
		ICP analysis	EDX	Surface area
$MoVAlO_x$-1	99	$Mo_1V_{0.15}Al_{0.20}O_x$	$Mo_1V_{0.26}Al_{0.11}O_x$	6
$MoVAlO_x$-2	96	$Mo_1V_{0.34}Al_{0.09}O_x$	$Mo_1V_{0.36}Al_{0.30}O_x$	16
$MoVAlO_x$-3	33	$Mo_1V_{0.7}Al_{0.28}O_x$	$Mo_1V_{0.78}Al_{0.69}O_x$	17
$MoVAlO_x$-4	13	$Mo_1V_{1.75}Al_{0.49}O_x$	$Mo_1V_{1.27}Al_{1.05}O_x$	17

[a] Yield of calcined catalysts, calculated on the basis of concentration of Mo with respect to initial elemental composition taken for the synthesis

the bulk except with the $MoVAlO_x$-4 catalyst indicating its mobility to the surface of the catalysts. BET surface area measurements have also been carried out for these catalysts and the data are presented in Table 1. The surface area of the catalyst $MoVAlO_x$-1 was 7 m^2/g while for the other catalysts, it was in the range 16–17 m^2/g.

3.1.2 Powder X-ray Diffraction

Figure 1 shows the powder XRD patterns of the four calcined catalysts prepared at different pH values. The calcination was carried out at 400 °C under N_2 after treating the catalysts in air upto 350 °C for 2 h. The catalysts $MoVAlO_x$-1 and $MoVAlO_x$-2 showed a similar XRD patterns exhibiting predominantly MoO_3 [JCPDS, 76-1003] and MoV_2O_8 [JCPDS, 74-1510] phases. Although, the quantification of different phases was not carried out, the relative intensity of MoO_3 is much higher in $MoVAlO_x$-1. Relative amount of MoV_2O_8 phase was higher in $MoVAlO_x$-2 compared to $MoVAlO_x$-1. In other words, the relative intensity ratio of $[MoV_2O_8]/[MoO_3]$ is higher in $MoVAlO_x$-2 than in $MoVAlO_x$-1. In addition, traces of Mo_4O_{11} [JCPDS, 13-0142], a reduced phase, is also seen in both catalysts (which is more prominent in $MoVAlO_x$-2). The XRD pattern of $MoVAlO_x$-3 exhibits MoV_2O_8 as a major phase along with a minor phase of $Mo_4V_6O_{25}$ [JCPDS, 34-0530]. Interestingly, MoO_3 phase is totally absent in $MoVAlO_x$-3. In addition, weak peaks seen at 2θ values 17.63(23)°, 29.51(15)°, 38.12(3)° and 46.19(12)° could not be fitted with any of the known single phases. For $MoVAlO_x$-4, the pattern was dominated by V_2O_5 [JSPDS, 85-0604] phase as a major phase along with a medium intensity Mo_4O_{11} and $MoVAlO_4$ [JSPDS, 89-0871] phases. A trace amount of $Mo_4V_6O_{25}$ phase was also seen in $MoVAlO_x$-4.

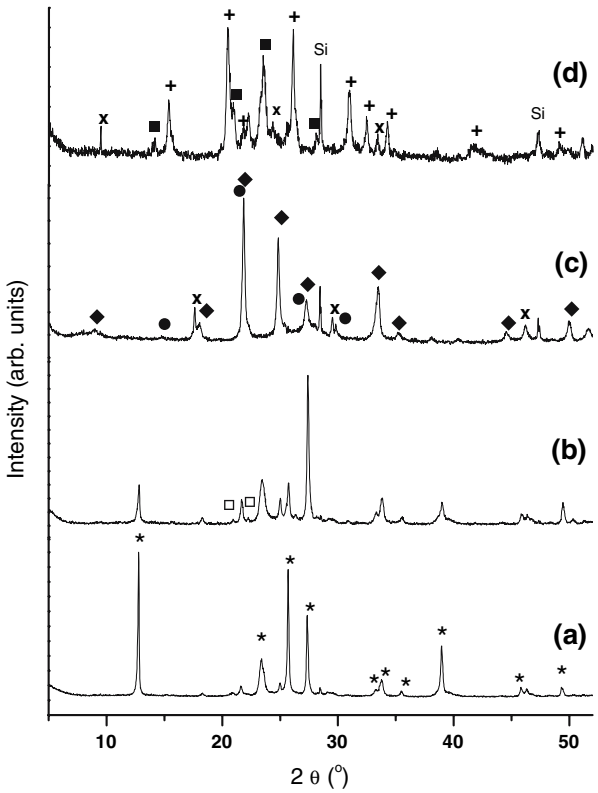

Fig. 1 Powder XRD pattern of the (**a**) $MoVAlO_x$-1, (**b**) $MoVAlO_x$-2, (**c**) $MoVAlO_x$-3 and (**d**) $MoVAlO_x$-4 catalysts. *: MoO_3, ♦: MoV_2O_8, □: Mo_4O_{11}, +: V_2O_5, ●: $Mo_4V_6O_{25}$, ■: $MoVAlO_7$, **x**: unidentified phase, Si: silicon standard

3.1.3 Morphology of $MoAlVO_x$ Catalysts

The morphology of calcined catalysts was investigated by SEM analysis. All the four catalysts were found to have completely different morphologies and the images are given in Fig. 2. Long rod or needle shaped crystals with a length about 4–40 μm were observed in the case of $MoVAlO_x$-1. These needle or rod-shaped crystals have collapsed into smaller sizes in $MoVAlO_x$-2 catalyst as shown in the Fig. 2. For the catalysts prepared at a higher pH values viz., $MoVAlO_x$-3 and $MoVAlO_x$-4, the images are more of microcrystalline and spongy in nature respectively.

3.1.4 Raman Spectroscopy

Raman spectroscopy was used to identify different moieties/phases having different coordination symmetry present in the catalytic catalysts. The Raman spectra of all the four calcined catalysts were recorded at room temperature and are shown in Fig. 3. The spectra of $MoVAlO_x$-1 and $MoVAlO_x$-2 catalysts showed bands at 992, 820, 664 cm^{-1} which are characteristic of α-MoO_3 species and its presence was also supported by the XRD data. A broad shoulder band around 700 cm^{-1} and a peak at 992 cm^{-1} (the latter band might be overlapped with that of α-MoO_3) indicate the presence of phases containing V_2O_5 unit viz. MoV_2O_8 phase [13]. Interestingly, for $MoVAlO_x$-3 and $MoVAlO_x$-4 catalysts, the intensity of 820 cm^{-1} band diminished to a weak and broad shoulder. However, the band centered around 700 cm^{-1} increased many fold and became a broader band for $MoVAlO_x$-4 catalyst. The above features indicate the absence or negligible amount of α-MoO_3 species and increased amount of pure V_2O_5/V_2O_5-containing phases e.g., MoV_2O_8 in these catalysts. This is quite understandable as the relative amount of vanadium content was higher in this catalyst compared to the catalysts prepared at a low pH. In the case of $MoVAlO_x$-4, the V content was more than that of Mo as seen in Table 1. The

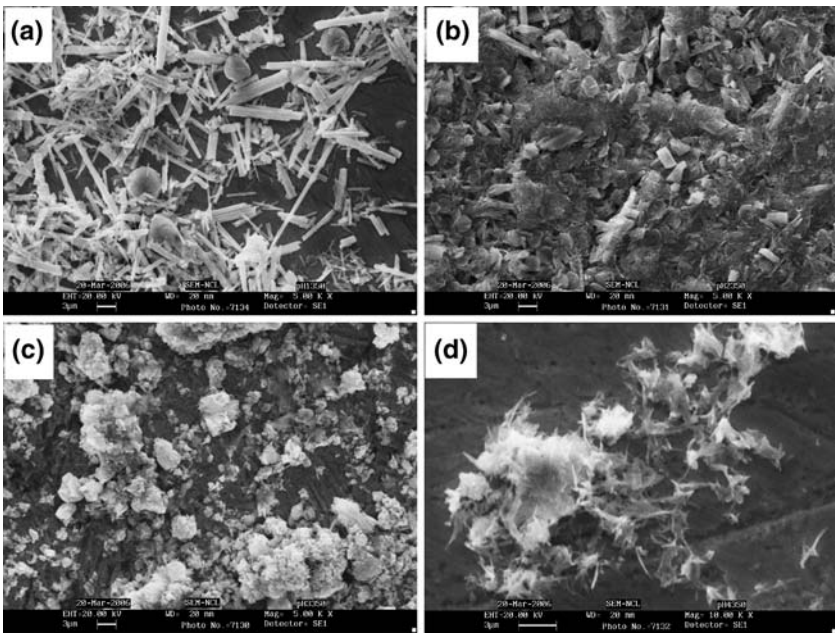

Fig. 2 SEM images of (**a**) $MoVAlO_x$-1, (**b**) $MoVAlO_x$-2, (**c**) $MoVAlO_x$-3 and (**d**) $MoVAlO_x$-4 catalysts

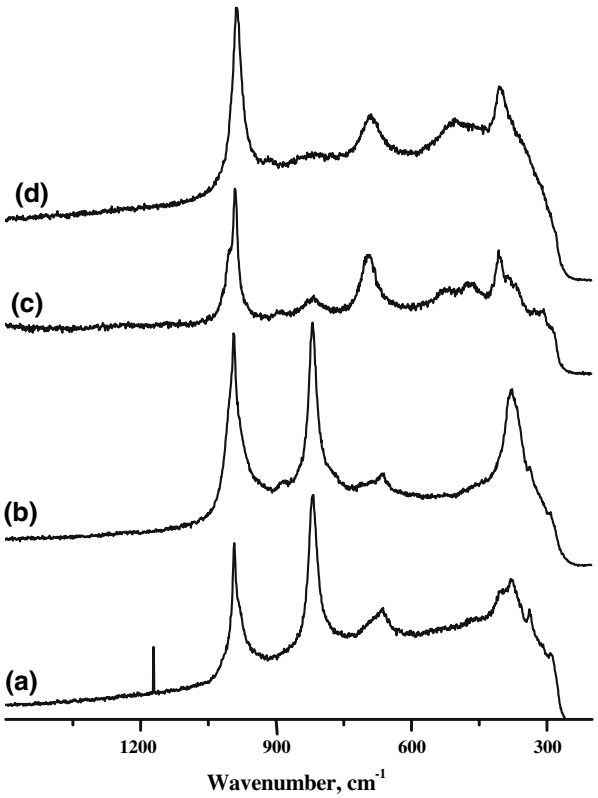

Fig. 3 Room temperature Raman spectra of (**a**) $MoVAlO_x$-1, (**b**) $MoVAlO_x$-2, (**c**) $MoVAlO_x$-3 and (**d**) $MoVAlO_x$-4 catalysts

bands at 900 and 850 cm^{-1} are generally attributed to the stretching mode of Mo–O–Mo bonds of polymerized surface molybdenum oxide containing species in different configurations (dimers, oligomers) [14, 15]. The broad bands centered around 920, 900 and 850 cm^{-1} are attributed to crystalline Mo_4O_{11} and $Mo_4V_6O_{25}$ species in addition to MoO_3-type compounds. The spectra of all catalysts showed a broad band in the region 700–675 cm^{-1} (which were stronger in $MoVAlO_x$-3 and $MoVAlO_x$-4) and a band around 400 cm^{-1}. These bands are assigned to V–O–V (V–O–Mo) stretching vibrations of polymeric surface species e.g., $MoVAlO_4$, $Mo_4V_6O_{25}$ etc. [16]. The bands can also be partly attributed to the presence of a bulk V_2O_5 especially for $MoVAlO_x$-4 catalyst as characteristic bands of V_2O_5 appear at 282, 405, 695 and 993 cm^{-1} [13]. The absence of 760 and 937 cm^{-1} bands in all the catalysts indicates that monomeric tetrahedral vanadate species ($\sim$760 cm^{-1}) and surface metavanadate species (937 cm^{-1}) are either absent or present in negligible quantities [17]. An isolated monovanadate group having terminal V=O stretching mode which generally exhibits a distinct narrow band at 1,030–1,020 cm^{-1}, is absent in the catalysts [13, 18]. Also, bands associated with $AlVO_4$ (characteristic bands are: 1,003, 970, 943 cm^{-1}) are absent in the calcined catalysts [19].

3.1.5 UV–Vis Spectroscopy

The diffuse reflectance UV–Vis spectra of the calcined catalysts prepared at different pH values were recorded at room temperature and reproduced in Fig. 4. The spectra were deconvoluted to identify different bands present especially in the region 200–500 nm. Accordingly, the spectra could be deconvoluted into five major bands centered around 234, 265, 307, 376, 452 nm and however, their intensities vary with catalysts prepared at different pH. The deconvoluted spectrum is given only for a typical $MoVAlO_x$-1 catalyst (in dashed lines). The UV–Vis spectra

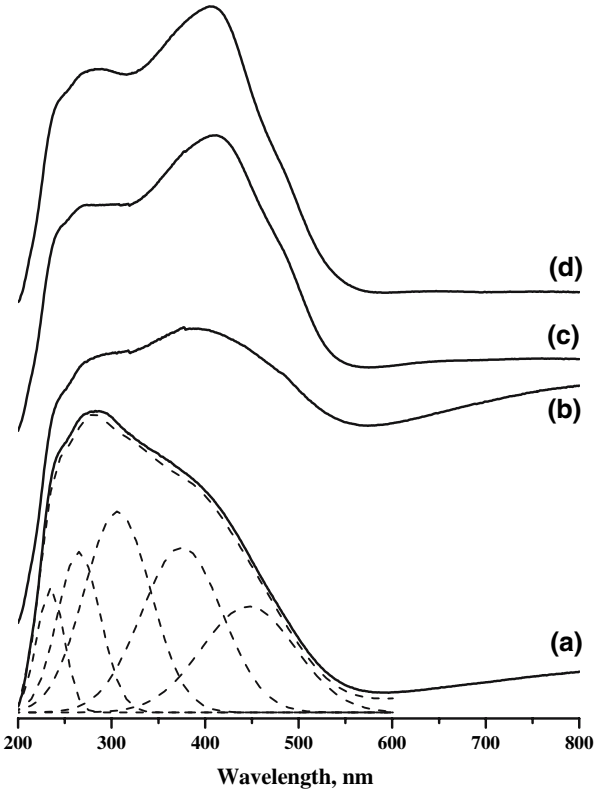

Fig. 4 Diffuse Reflectance UV–Vis spectra of (**a**) $MoVAlO_x$-1, (**b**) $MoVAlO_x$-2, (**c**) $MoVAlO_x$-3 and (**d**) $MoVAlO_x$-4 catalysts. Deconvolution of UV–Vis spectrum of $MoVAlO_x$-1, is given in dashed lines. Deconvolution of the other spectra are nearly same except for the intensity of individual bands and are not shown for clarity

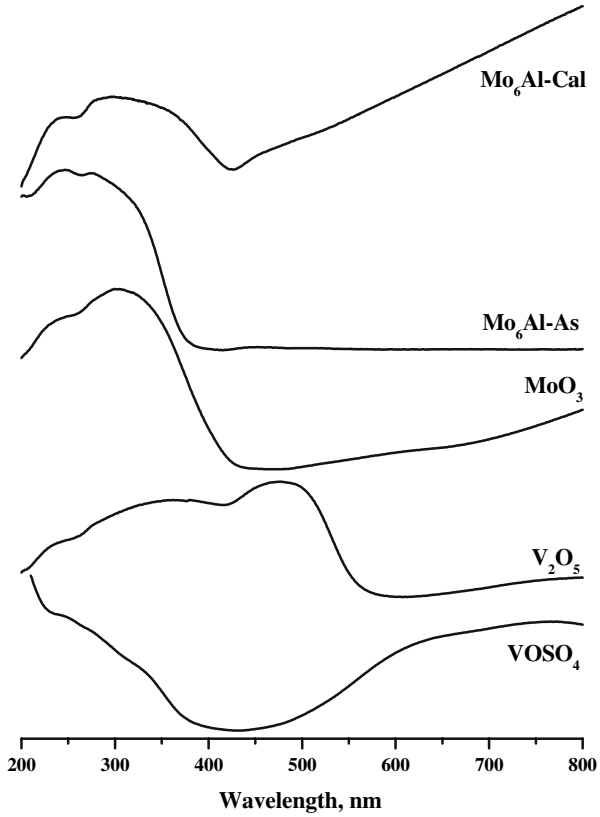

Fig. 5 Diffuse Reflectance UV–Vis spectra of different standard catalysts

of few reference catalysts namely $VOSO_4$, V_2O_5, MoO_3 and as-synthesized and calcined $(NH_4)_3AlMo_6H_6O_{24} \cdot 7\ H_2O$ catalysts, represented as Mo_6Al–As and Mo_6Al–Cal, respectively, were also recorded for a comparison and the spectra are given in Fig. 5.

The UV–Vis spectra of all the calcined catalysts were dominated by five major peaks centered around 234, 265, 307 (br), 376, 452 (vs) nm and also a broad band above 500 nm. The intensity of the bands centered around 234, 265 and 307 nm were more strong and the peaks at 376 and 452 nm appeared as a shoulder for $MoVAlO_x$-1 catalyst. While the relative intensity of 234 and 265 nm bands are more or less same for both $MoVAlO_x$-2 and $MoVAlO_x$-1, bands in the region 305–480 nm became stronger for $MoVAlO_x$-2. The features of $MoVAlO_x$-3 and $MoVAlO_x$-4 were almost similar and the bands in the region 305–480 nm became more intense and a broad shoulder at 452 nm became clearly visible.

The bands in the range of 230–310 nm present in all the catalysts were assigned to Mo^{6+} in octahedral coordination with different structural arrangement [5, 17, 18, 20]. The above assignment was further substantiated by the UV–Vis spectra of the reference catalysts namely MoO_3, Mo_6Al–As and Mo_6Al–Cal catalysts (Fig. 5) and their spectra are dominated by characteristic bands in the region 200–350 nm. The broad bands appeared above 550 nm are assigned to a *d–d* band associated with Mo and V ions with lower oxidation states e.g., Mo^{5+}/Mo^{4+} or V^{4+} as they are expected to exhibit bands in the region 400–750 cm^1 [21]. The above assignments were further supported by comparing the spectra of reference samples, Mo_6Al–Cal and $VOSO_4$, which have a substantial amount of Mo^{5+} and V^{4+}, respectively, showing characteristic of *d–d* band above 500 nm. The dominant band centered around 376 nm in all the calcined catalysts were assigned to penta coordinated V^{5+} [5, 17, 18]. The assignment was also confirmed by comparing with the UV–Vis spectrum of reference V_2O_5 catalyst where the vanadium is in five coordination state. The intensity of the above band increases at higher pH values due to the increase in V content at higher pH.

3.1.6 EPR Spectroscopy

Figure 6 shows the EPR spectra of all the four calcined catalysts were recorded at room temperature. While the EPR spectra of $MoVAlO_x$-1 and $MoVAlO_x$-2 catalysts

showed overlapped signals corresponding to Mo^{5+} and V^{4+}, $MoVAlO_x$-3 and $MoVAlO_x$-4 catalysts gave signals corresponding to mainly of Mo^{5+} with no trace of V^{4+}signal. The EPR spectra of V^{4+} centers are characteristic of an axial symmetry typical for orthogonal geometry [22]. The EPR spectra of V^{4+} of $MoVAlO_x$-1 and $MoVAlO_x$-2 were best fitted with Hamiltonian parameters, $g_{\|} = 1.926$, $g_{\perp} = 1.985$, $A_{\|} = 183$ G, $A_{\perp} = 53$ at operating microwave frequency, 9.457 GHz. A representative simulated spectrum is given in Fig. 6 in dotted lines for the catalyst $MoVAlO_x$-2. Normalization of the simulated spectrum with the parallel components of V^{4+} EPR signal clearly showed that EPR spectra of $MoVAlO_x$-1 and $MoVAlO_x$-2 consist of overlapped signals from V^{4+} and Mo^{5+} species. EPR of Mo^{5+} showed unresolved broad isotropic-like pattern (peak-to-peak line-width of 90 G). The assignment of the EPR signal to Mo^{5+} was also substantiated by that of the reference catalyst, Mo_6Al–Cal, which showed a characteristic Mo^{5+} signal with 70 G line-width (Fig. 6). The broad line width may be due to the presence of more than one Mo^{5+} sites and/or due to magnetic interactions between the paramagnetic Mo^{5+} centers which are in close proximity.

In order to quantify the amount of paramagnetic centers viz., V^{4+} and Mo^{5+}, with respect to the total V and Mo contents respectively, the area under the peak of all the EPR spectra (double integration) was calculated using vanadyl sulphate as a standard. Accordingly, V^{4+}/V_{total} was estimated to be around 0.8% in $MoVAlO_x$-1 and $MoVAlO_x$-2 whereas Mo^{5+}/Mo_{total} was around 2.5% for all the catalysts indicating that the majority of Mo and V species are in their higher oxidation states namely 6+ and 5+, respectively which are diamagnetic. For $MoVAlO_x$-1 and $MoVAlO_x$-2 catalysts, area corresponding to V^{4+} was determined separately based on the simulation before estimating the Mo^{5+} content.

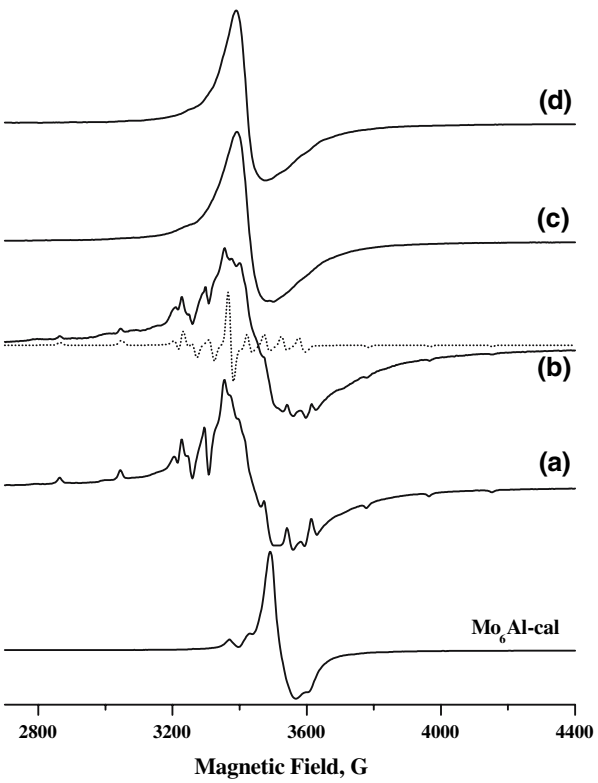

Fig. 6 Room temperature EPR spectra of (**a**) $MoVAlO_x$-1, (**b**) $MoVAlO_x$-2, (**c**) $MoVAlO_x$-3, (**d**) $MoVAlO_x$-4 catalysts and Mo_6Al–Cal catalyst

3.2 Selective Oxidation of Ethane

All the four catalysts were tested for selective oxidation of ethane in a fixed bed reactor as described in the experimental section. The reaction was carried out typically at the experimental condition of 300 °C and 15 bar with a flow rate of 48.33 mL/min using ethane/air/steam: 27.6/47.6/24.8 mol% over 2 g of catalyst loading. The reaction was allowed to run for several hours ($\sim$10 h) to attain a saturation and then the products were analyzed for every 3 h and the results are summarized in Table 2. Each data point is an average of three measurements. In all these cases, acetic acid and ethylene were the main products apart from CO and CO_2. Other products like ethanol, methanol and acetaldehyde were also seen but in less than 150 ppm level and are not discussed further. As seen in Table 2, $MoVAlO_x$-1 gave 30 mol% selectivity to acetic acid and 32 mol% selectivity to ethylene at the ethane conversion of 9.7 mol%. Interestingly, $MoVAlO_x$-2 showed an excellent activity with 23 mol% ethane conversion with a combined ethylene and acetic acid selectivity of 80.6 mol% where acetic acid selectivity alone was 40.2 mol%. $MoVAlO_x$-3 showed a moderate ethane conversion (10.5 mol%) with a better acetic acid selectivity of 46 mol% where the combined ethylene and acetic acid selectivity of 82 mol%. In both $MoVAlO_x$-2 and $MoVAlO_x$-3 catalysts, the selectivity to CO and CO_2 was very low. The catalyst $MoVAlO_x$-4 showed the least activity of 8.2 mol% ethane conversion with lowest acetic acid selectivity of 3 mol% where selectivity to ethylene was 18 mol% and selectivity to CO_x was 79 mol%. $MoVAlO_x$-2 gave highest acetic acid yield of 9.25 mol% while $MoVAlO_x$-4 gave the least yield (0.25 mol%). The other catalysts viz., $MoVAlO_x$-1 and $MoVAlO_x$-3 gave an acetic acid yield of 2.91 and 3.78 mol% respectively as shown in Table 2.

Since $MoVAlO_x$-2 showed a better activity towards ethane oxidation than the other catalysts, $MoVAlO_x$-2 catalyst was alone tested at different experimental conditions to understand their effects on the ethane conversion and the products selectivity. Experiments were carried out

Table 2 Selective oxidation of ethane over $MoVAlO_x$ catalysts prepared at different pH values

Catalyst	Ethane conversion (mol %)	Product selectivity (mol%)				CH_3COOH yield (mol %)
		CH_3COOH	CH_2CH_2	CO	CO_2	
$MoVAlO_x$-1	9.7	30	32	19	19	2.91
$MoVAlO_x$-2	23	40.2	40.4	11.6	7.8	9.25
$MoVAlO_x$-3	10.5	36	46	10	8	3.78
$MoVAlO_x$-4	8.2	3	18	9	70	0.25

Pretreatment temperature: 400 °C for 4 h in He stream (20 mL/min). Reaction conditions: temperature, 300 °C, pressure, 15 bar, catalyst, 2 g, flow rate of 48.33 mL/min, ethane/air/steam: 27.6/47.6/24.8 mol%. Acetic acid yield: conversion × selectivity

at different reaction pressures in the range 5–20 bar with a feed of ethane/air/steam: 27.6/47.6/24.8 mol% at reaction temperature 300 °C and the results are plotted in Fig. 7. The reaction pressure has a definite influence on ethylene and acetic acid selectivity. As seen in the Figure, there is a gradual increase in the ethane conversion with increase in the reaction pressure and reached nearly a plateau above 15 bar pressure. The ethane conversion was around 8% at 5 bar and increased to 23% at 15 bar. The acetic acid selectivity was around 20% and the ethylene selectivity was around 73% at 5 bar and both reached around 40% at

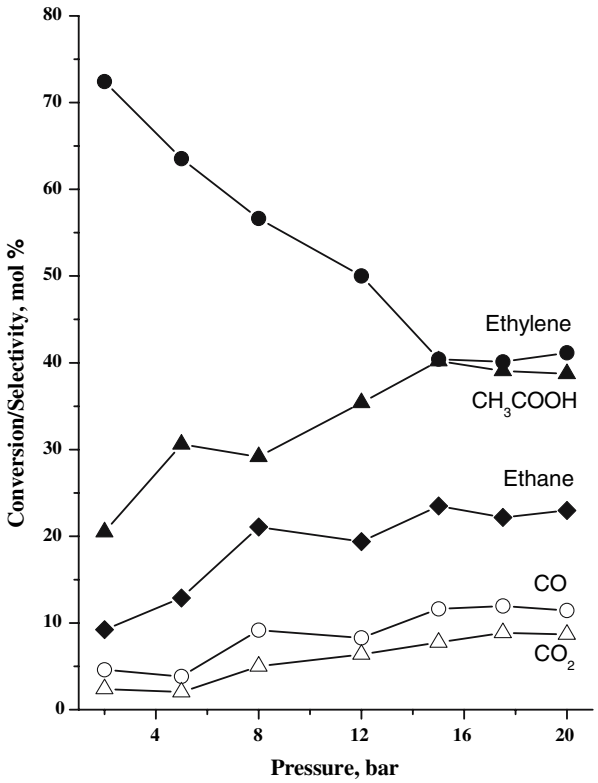

Fig. 7 Conversion and selectivity profiles on selective oxidation of ethane over $MoVAlO_x$-2 catalyst w.r.t. reaction pressure. Pretreatment temperature: 400 °C for 4 h in He stream (20 mL/min). Reaction conditions: temperature, 300 °C, catalyst, 2 g, flow rate of 48.33 mL/min, ethane/air/steam: 27.6/47.6/24.8 mol%

15 bar pressure and thereafter, the selectivity of ethylene and acetic acid were more or less the same until 20 bar pressure. Thus, the optimum reaction pressure was around 15 bar at 300 °C. The variation in the selectivity to CO and CO_2 were small as compared to that of ethylene and acetic acid where the selectivity to CO was slightly higher than that of CO_2. Selectivity to CO was around 5% at 5 bar which reached around 11% at 20 bar and CO/CO_2 mole ratio remained around 1.6 ± 0.4 throughout the pressure range employed.

At an optimum reaction pressure of 15 bar with a feed composition of ethane /air/steam: 27.6/47.6/24.8 mol%, oxidation experiments were carried out at different reaction temperatures in the range of 260–340 °C. The variation in the selectivity of ethylene, acetic acid, CO and CO_2 along with the ethane conversion as a function of temperature is shown in Fig. 8. The ethane conversion at 270 °C was 5% and increased to 27 mol% at 340 °C. Although the combined selectivity to ethylene and acetic acid was around 80% throughout the temperature range employed, the acetic acid selectivity decreased from 44 to 36% on increasing the temperature from 260 to 340 °C. On the other hand, the trend for ethylene selectivity was reverse with increase in temperature. The other products were namely CO and CO_2 increase with temperature due to the combustion reactions of ethylene and acetic acid. The CO selectivity was slightly higher than that of CO_2 as shown in the figure [23].

The time on stream study was carried out with $MoVAlO_x$-2 catalyst to test the stability and activity of the catalyst with time. The reaction was carried out for 50 h and was monitored at regular time intervals at 300 °C and 15 bar with the feed: ethane/air/steam: 27.6/47.6/24.8 mol%. The profile of ethane conversion and the product selectivity with time is given in Fig. 9 where each data point was the average of three experiments.

The influence of addition of water (steam) co-feed on the ethane conversion and the product selectivity was studied at the reaction temperature, 300 °C by varying the partial pressure of water at a constant partial pressure of ethane and oxygen. The ethane conversion and selectivity

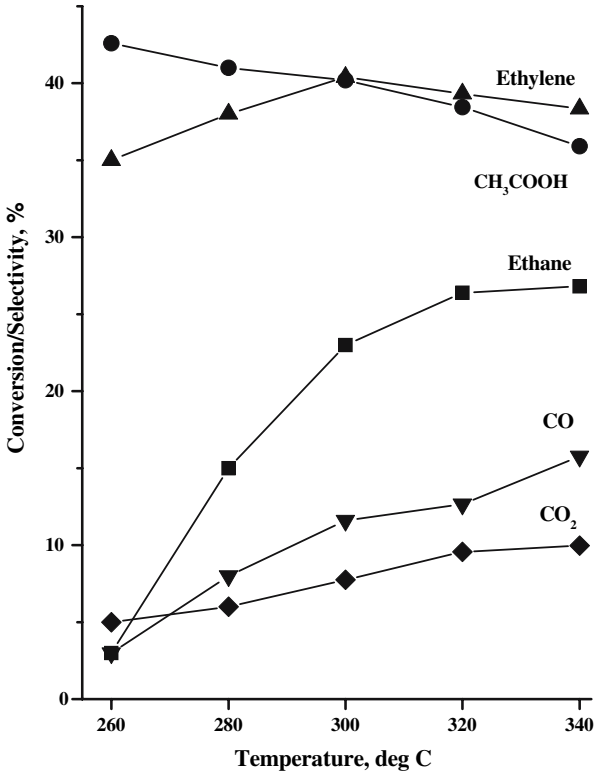

Fig. 8 Conversion and selectivity profiles on selective oxidation of ethane over $MoVAlO_x$-2 catalyst w.r.t reaction temperature. Pretreatment temperature: 400 °C for 4 h in He stream (20 mL/min). Reaction conditions: pressure, 15 bar, catalyst, 2 g, flow rate of 48.33 mL/min, ethane/air/steam: 27.6/47.6/24.8 mol%

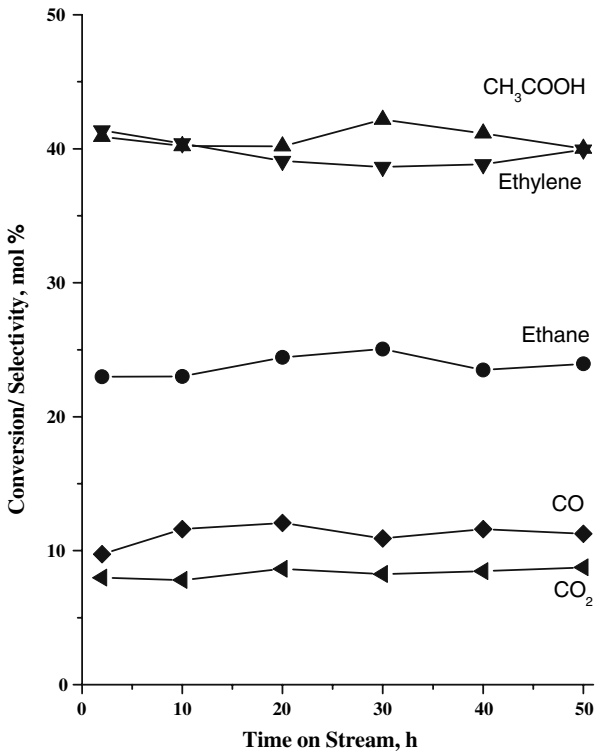

Fig. 9 Time on stream study of selective oxidation of ethane over $MoVAlO_x$-2 catalyst w.r.t. reaction temperature. Pretreatment temperature: 400 °C for 4 h in He stream (20 mL/min). Reaction conditions: temperature, 300 °C, pressure, 15 bar, catalyst, 2 g, flow rate of 48.33 mL/min, ethane/air/steam: 27.6/47.6/24.8 mol%

of the products namely acetic acid, ethylene and CO_2 are shown in Fig. 10 as a function of partial pressure of water. The experiment was performed by varying the partial pressure of water between 1.55 and 6.23 bar at a constant total pressure of 15 bar at the reactor inlet where the partial pressure of ethane was 3.22 bar and that of oxygen was 5.625 bar (balance by nitrogen). As shown in the Figure, the conversion of ethane decreases gradually from 23.8 to 16.1 mol% when the partial pressure of water was increased from at 1.55 to 6.23 bar. Addition of steam showed a positive influence on the acetic acid selectivity as the acetic acid selectivity increased from 36.1 mol% at 1.33 bar to 43.9% at 6.23 bar partial pressure of water whereas ethylene selectivity showed an opposite trend, 41.8% at 1.33 bar and 37% at 6.23 bar. The CO_2 selectivity was almost constant for the entire range of water partial pressure where CO was seen only as a trace.

4 Discussion

Although the initial preparative elemental compositions were same, the pH at which the catalysts were made has a strong influence on the bulk and surface elemental compositions and the catalyst yield. Decreasing trend of Mo/V and Mo/Al ratios with increase in pH (Table 1) indicates that Mo content in the catalysts decreases with increase in the pH value. Also, the yield of the calcined catalysts decreased with increase in pH. The decrease in the Mo content and the catalyst yield should be associated with the higher solubility of Mo or dissociation of Anderson heteropoly compound, $(NH_4)_3AlMo_6H_6O_{24} \cdot 7\ H_2O$, at higher pH which creates a less favorable situation for the formation of mixed metal oxides with the expected elemental composition. Thus, the pH of the slurry has a profound effect on the nature of the precursors and their amount available for the formation of mixed metal oxide catalysts at the hydrothermal condition and also on the formation of crystalline phases during the heat treatment as seen in the powder XRD patterns. While the surface area in the range 7–20 m^2/g is typical for the mixed metal oxide catalysts, observed lower surface area of $MoVAlO_x$-1 should be due to its high crystalline nature [7].

The powder XRD patterns of the present $MoVAlO_x$ catalysts are different from that of the reported $MoVAlO_x$ having a similar elemental composition [24]. The reported XRD pattern of $MoVAlO_x$ showed mainly two sharp peaks at 22 and 45° (*00l*) reflections along with other diffractions

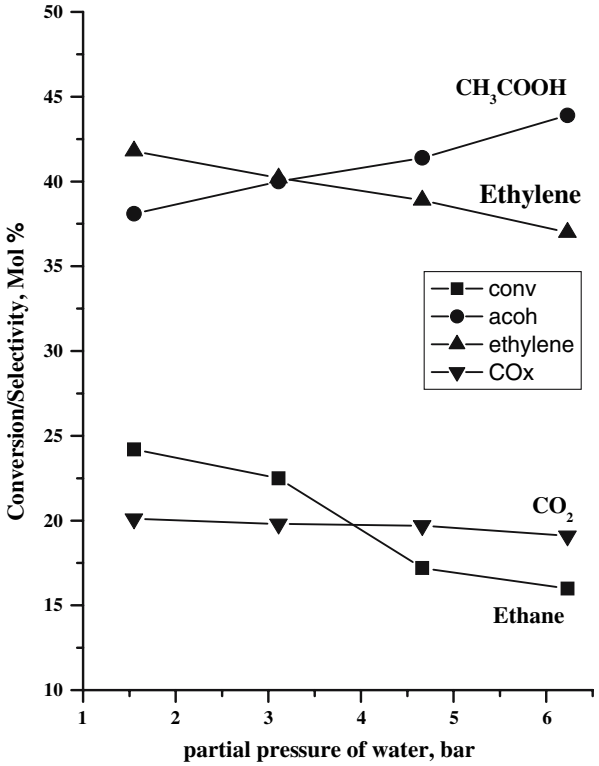

Fig. 10 Effect of partial pressure of water on the ethane conversion and product selectivity during selective oxidation of ethane over $MoVAlO_x$-2 catalyst. Experimental conditions: temperature, 300 °C, total pressure, 15 bar, catalyst, 2 g, PO_2 = 5.625 bar and PC_2H_6 = 3.22 bar, the partial pressure of water was varied between 1.55 and 6.23 bar, total pressure = 15 bar

at lower angles. The presence of strong peak line at 22° (d = 4 Å) was reported to be responsible for the good catalytic activity of the catalyst. However, with the present catalyst systems the peak at 22° 2θ is not strong. The difference in the XRD patterns of the present catalysts from the reported one may be attributed to the pH condition of the preparative composition and subsequent temperature treatments. All the four as-synthesized catalysts prepared at different pH values were calcined under the identical conditions i.e. heating upto 350 °C under static air and then to 400 °C under the N_2 atmosphere. α-MoO_3 phase which is present in $MoVAlO_x$-1 and $MoVAlO_x$-2, is totally absent in the other two catalysts prepared at higher pH values. Thus, the present results show that the amount of MoO_3 can be controlled by pH of the initial preparative slurry. The presence of high amount of V_2O_5 in $MoVAlO_x$-4, MoO_3 in $MoVAlO_x$-1 and different elemental compositions at different pH conditions indicate that presence of the right amount of different elements during the temperature treatment is highly important for the formation of active species. It is generally observed that presence of additional metal ion like Nb to $MoVO_x$-basic composition influences formation of partially reduced phase (Mo_4O_{11}-type) and decreases the formation of MoO_3 [25]. It appears that in the present catalyst systems, Al ion plays a role of Nb in stablising different active phases. Although Al containing phases are not observed except in $MoVAlO_x$-4, Al might have been incorporated in vanadomolybdate or highly dispersed on the other phases, owing to its low content such that it is not seen in XRD pattern or it existed in an amorphous state.

A partial reduction of the catalysts with a temperature treatment is generally observed in the presence of oxalate and nitrate anions in the catalyst precursors [4, 26]. In some cases, the presence of NO_x favors partial oxidation of metal ions with a enhanced activity [27]. Although neither oxalate nor nitrate salts were used in the present catalyst systems, observed partial reduction of Mo^{6+} to Mo^{5+} might be due to ammonium ions present. The observation of EPR signal upon the heat treatment of a diamagnetic Mo_6Al–As precursor substantiates the point that ammonium ions present in the precursor is responsible for the partial reduction of Mo^{6+}. Estimation of amount of V^{4+} and Mo^{5+} in the calcined catalysts showing $V^{4+}/V_{total} = \sim 0.8$ % and $Mo^{5+}/Mo_{total} \sim 2.5\%$ indicated that majority of Mo and V are in their higher oxidation states, viz., 6+ and 5+, respectively which are diamagnetic. It may also be noted here that any paramagnetic centers connected through a super-exchange pathway leading to strong anti-ferromagnetic interactions might not have contributed for the EPR intensity. Presence of such anti-ferromagnetic interactions in the present cases can not be ruled out.

While all the catalysts prepared at different pH values were found to be active for the ethane oxidation as seen in the Table 1, the catalysts prepared at pH 1, 2 and 3 showed better selectivity to ethylene and acetic acid with a moderate ethane conversion. Based on the phases identified from the powder XRD, it appears that the MoV_2O_8 phase, which is present in the catalysts prepared at pH 1–3 might be responsible for the selective oxidation of ethane to acetic acid/ethylene. The XRD patterns of both $MoVAlO_x$-1 and $MoVAlO_x$-2 are nearly similar except for the fact that (*020*) reflection of MoO_3 is very strong (100%) in $MoVAlO_x$-1 as compared to $MoVAlO_x$-2. The above observation is likely due to the preferential orientation of the MoO_3 crystals in $MoVAlO_x$-1. The superior activity of $MoVAlO_x$-2 compared to $MoVAlO_x$-1 needs further investigation. The higher ratio of MoV_2O_8/MoO_3 in $MoVAlO_x$-2 compared to $MoVAlO_x$-1 may be due to the lower Mo/V ratio in $MoVAlO_x$-2. As seen in the elemental analysis data (Table 1) the Mo:V ratio was 1:0.15 in $MoVAlO_x$-1 compared to 1:0.34 in $MoVAlO_x$-2. The presence of MoV_2O_8 and $Mo_4V_6O_{25}$ in $MoVAlO_x$-3 and its moderate activity substantiate the conclusion that MoV_2O_8 might be an important phase responsible for the catalytic activity. The higher ethane conversion with the $MoVAlO_x$-2 catalyst compared to the $MoVAlO_x$-3 catalyst indicates

that MoO_3 support is important for the better activity. Apart from MoV_2O_8/MoO_3 ratio, the amount of the reduced phase Mo_4O_{11} was higher in $MoVAlO_x$-2 compared to $MoVAlO_x$-1 indicating the possibility that the MoV_2O_8 phase along with the reduced species may be important for the excellent activity. With the above background, it is easy to understand the least catalytic activity of $MoVAlO_x$-4 catalyst where MoV_2O_8 and Mo_4O_{11} phases are minor phases and MoO_3 phase was totally absent. Presence of V_2O_5 and other high vanadium-containing phases like $MoVAlO_4$ might be responsible for the over oxidation of the formed product namely ethylene and acetic acid.

It may be noted here that the partial reduction of catalyst precursors has been reported to have a positive influence on the activity and selectivity in selective oxidation of the lower alkanes, though the exact role of these species are yet to be understood [4, 25, 26]. The presence of reduced species with V^{4+} centers in $MoVAlO_x$-1 and $MoVAlO_x$-2 catalysts and Mo^{5+} in $MoVAlO_x$-3 and $MoVAlO_x$-4 catalysts is obvious from EPR results though the amount may be low. However, the nature and location of V^{4+} is not clear from the present study. One possibility is that part of vanadium ion in MoV_2O_8 is in 4+ oxidation state as MoV_2O_8 is the only vanadium containing crystalline phase in $MoVAlO_x$-1 and $MoVAlO_x$-2. However, the absence of V^{4+} EPR signal in $MoVAlO_x$-3 where MoV_2O_8 phase is the major phase, indicates that presence of V^{4+} containing non-crystalline species can not be ruled out. Presence of Mo^{5+} and other reduced phases containing Mo^{5+} are clear from EPR, UV–Vis and XRD data.

The best results of the ethane oxidation with the present catalytic system ($MoVAlO_x$-2) are compared with that of other catalytic systems known in the open literature in Table 3. The data are selected such that the reaction temperature is less than 600 °C. It is clear from the table that suitable combination of metal ions, their composition, method of preparation and the appropriate reaction conditions play a crucial role in achieving decent ethylene and acetic acid yields.

Authors believe that ethane is converted to ethylene by oxidative dehydrogenetion mechanism which in-turn is adsorbed back on the catalyst to form acetic acid. Decrease in the acetic acid selectivity and increase in the ethylene selectivity on increasing the temperature is believed to be associated with adsorption and desorption phenomena. At high temperatures, the energy, kT (where k is Boltzmann constant) was enough to desorb the ethylene and thus making it not available for the acetic acid formation. The time on stream studies indicated that the catalyst is stable and active for several hours without any deactivation. Commonly occurring catalyst deactivation by coking is not expected in the present systems due to the oxidative experimental conditions.

The studies of the effect of partial pressure of water co-feed on ethane oxidation indicated that the water co-feed has a positive influence on the acetic acid selectivity and negative influence on the ethylene selectivity and the ethane conversion rate. The positive influence of steam on the acetic acid selectivity is believed to be associated with the hydroxyl group formation on the surface of catalyst which in turn facilitates the conversion of ethylene to acetic acid [34–36]. A reduction in the rate of ethane oxidation by water co-feed has been observed by others for various metal oxide systems [2, 8, 34]. The decrease of ethane conversion might be associated with adsorption of strong polar substrate like water and/or acetic acid, thus, blocking the active sites that lead to the reduction of the ethane oxidation rate. Different effect of water co-feed on the formation of acetic acid and CO_2 indicates the possibility

Table 3 Selective oxidation of ethane over metal oxide catalysts

Catalyst	Temp (°C)	Press (bar)	C_2H_6 Conv (mol %)	Selectivity (mol %)		Ref
				Ethylene	AcOH	
$Mo–V–Nb–O_x$	200	atm	2.3	0	100	[28]
V/TiO_2	225	atm	0.5		73	[29]
$Mo_6V_1Al_1O_x$	340	atm	1.8	72.9	12.4	[9, 30]
$Mo_6V_2Ga_1O_x$	340	atm	5.6	69.0	3.2	[30]
$Mo_6V_2Bi_1O_x$	340	atm	3.5	69.2	5.2	[30]
$Mo_6V_2Sb_1O_x$	340	atm	16.8	74.7	1.1	[30]
$Mo_6V_2Te_1O_x$	340	atm	18.2	72.5	2.5	[30]
VO_x/γ-Al_2O_3	575	atm	64	28	–	[31]
VO_x/TiO_2	325	atm	10.1	30.7	0.1	[32]
$Mo_1V_{0.18}Sb_{0.15}O_x$	400	atm	64.6	81.5	–	[33]
$Mo_1V_{0.25}Nb_{0.12}Pd_{0.0005}O_x$	246	15	4.7	21	47	[2]
$Mo_1V_{0.34}Al_{0.16}O_x$–pH2	300	1	9.1	74.5	18.1	Present work
$Mo_1V_{0.34}Al_{0.16}O_x$–pH2	300	15	23	40.4	40.2	Present work

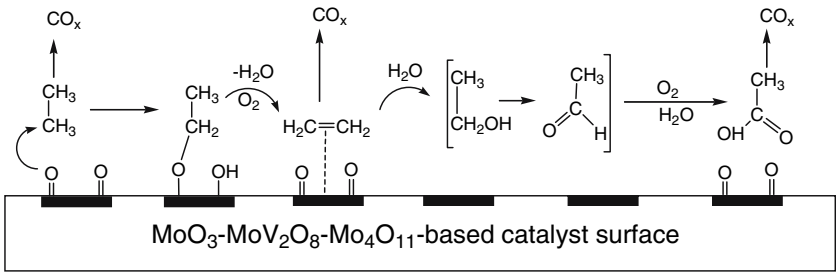

Fig. 11 Tentative reaction scheme and surface mechanism for the ethane oxidation to ethylene and then to acetic acid. Selective active sites are schematically represented as dark rectangular box

for different types of sites where water seems to be preferentially interacting on the site that is responsible for ethylene to acetic acid formation.

Based on the information obtained with the present investigation, although it is difficult to formulate exact reaction mechanism, a tentative surface mechanism for the oxidative dehydrogenation of ethane over $MoVAlO_x$ based catalysts is given in Fig. 11. The efficiency of the present catalyst system for the selective ethane oxidation is assumed to be due to the presence of MoV_2O_8 and other reduced species supported the MoO_3 phase. Activation of the C–H bond of ethane on the catalytic surface possibly via unstable ethoxy intermediate leads to ethylene formation. Part of the formed ethylene adsorb either weakly or strongly on the selective site of the catalyst surface in the presence of water and oxygen that leads to formation of intermediates like ethanol and acetaldehyde and finally to acetic acid. Although alcohol/aldehyde products were not seen as major products, their concentration upto 150 ppm were detected in the GC analysis. With the present experimental conditions, oxidation rate of these alcohol/aldehyde intermediates leading to acetic acid might be very high. Any of these intermediates, ethane and/or acetic acid will be oxidized to CO_x, if they are strongly adsorbed on any non-selective phase (e.g., alumina or V_2O_5). Desorption of ethylene will be easier if it is bound on weak acid like MoO_3 site.

5 Conclusions

The final elemental compositions of the catalysts having general formula $MoVAlO_x$, which were prepared with the same initial elemental composition, were found to be highly pH dependent. The catalyst prepared at pH 2 showed excellent activity for the selective oxidation of ethane with 23% ethane conversion and 80.6% combined selectivity to ethylene and acetic acid, and the catalyst prepared at pH4 showed least activity. Based on the XRD and Raman, UV–Vis and EPR studies, the higher activity has been attributed to the presence of MoV_2O_8 and other reduced species like Mo_4O_{11} phases supported on MoO_3 phase. The presence of V and Mo ions in partially reduced form seems to play a crucial role in the selective oxidation of ethane. While the excess of steam co-feed enhances the acetic acid selectivity, it retards the ethane conversion rate.

Acknowledgments The authors thank Council of Scientific and Industrial Research (CSIR), New Delhi, India for the financial support under New Millenium Indian Technology Leadership Initiative (NMITLI) program. We thank Dr. S. Sivasanker for all his invaluable support and encouragement. RHI thanks University Grant Commission (UGC), New Delhi for the fellowship. We thank Dr. K. V. G. K. Murty, AU-KBC Research Center, Anna University, India for Raman measurements.

References

1. Vitry D, Morikawa Y, Dubois JL, Ueda W (2003) Appl Catal A 252:411
2. Linke D, Wolf D, Baerns M, Timpe O, Schlögl R, Zeyβ S, Dingerdissen U (2002) J Catal 205:16
3. Lin MM (2001) Appl Catal A 207:1
4. Oliver JM, Nieto JML, Botella P, Mifsud A (2004) Appl Catal A 257:67
5. Smejkal Q, Linke D, Baerns M (2005) Chem Eng Proc 44:421
6. Nieto JML, Botella P, Vázquez MI, Dejoz A (2002) Chem Commun 1906
7. Roussel M, Bouchard M, Karim K, Al-Sayari S, Bordes-Richard E (2006) Appl Catal A 308:62
8. Heracleous E, Lemonidou AA (2006) J Catal 237:175
9. Oshihara K, Hisano T, Ueda W (2001) Topics Catal 15:153
10. Asakura K, Nakatani K, Kubota T, Iwasawa Y (2000) J Catal 194:309
11. Ueda W, Chen NF, Oshihara K (1999) Chem Commun 517
12. Nomiya K, Takahashi T, Shirai T, Miwa M (1987) Polyhedron 6:213
13. Khodakov A, Olthof B, Bell AT, Iglesia E (1999) J Catal 181:205
14. Dieterle M, Mestl G, Jäger J, Uchida Y, Hibst H, Schlögl R (2001) J Mol Catal A 174:169
15. Mestl G, Linsmeier Ch, Gottschall R, Dieterle M, Wild U, Schlögl R (2000) J Mol Catal A 162:463
16. Daniell W, Ponchel A, Kuba S, Anderle F, Weingand T, Gregory DH, Knozinger H (2002) Topics Catal 20:65
17. Jehng JM, Wachs IE, Clark FT, Springman MC (1993) J Mol Catal 81:63
18. Heracleous E, Machli M, Lemonidou AA, Vasalos IA (2005) J Mol Catal A 232:29
19. Kanervo JM, Harlin ME, Krause AOI, Bañares MA (2003) Catal Today 78:171
20. Oliver JM, Nieto JML, Botella P (2004) Catal Today 96:241
21. Davidson A, Che M (1992) J Phys Chem 96:9909
22. García-González E, López Nieto JM, Botella P, González-Calbet JM (2002) Chem Mater 14:4416

23. Heracleous E, Lemonidoua AA, Lercher JA (2004) Appl Catal A: Gen 264:73
24. Oshihara K, Nakamura Y, Sakuma M, Ueda W (2001) Catal Today 71:153
25. Roussel M, Bouchard M, Bordes-Richard E, Karim K, Al-Sayari S (2005) Catal Today 99:77
26. Tsuji H, Koyasu Y (2002) J Am Chem Soc 124:5608
27. Gaffney AM, Heffner MD, Song R (2002) EP 1249274
28. Thornsteinson EM, Wilson TP, Young FG, Kasai PH (1978) J Catal 52:116
29. Tessier L, Bordes E, Gubelmann-Bonneau M (1995) Catal Today 24:335
30. Ueda W, Oshihara K (2000) Appl Catal A 200:135
31. Klose F, Joshi M, Hamel C, Morgenstern AS (2004) Appl Catal A 260:101
32. Enache DI, Bordesc E, Ensuque A, Verduraz FB (2004) Appl Catal A 278:103
33. Botella P, Dejoz A, Lopez Nieto JM, Concepción P, Vázquez MI (2006) Appl Catal A 298:16
34. Argyle MD, Chen K, Bell AT, Iglesia E (2002) J Phys Chem B 106:5029
35. Evnin AB, Rabo JA, Kasai PH (1973) J Catal 30:109
36. Seoane JL, Boutry P, Montarnal R (1980) J Catal 63:191
37. Zeyss S, Dingerdissen U, Fritch J (2004) US Patent 6,790,983